What controls the uptake of transient tracers in the Southern Ocean?

Takamitsu Ito, John Marshall, and Michael Follows

Program in Atmospheres, Oceans and Climate, Department of Earth Atmospheric and Planetary Sciences, Massachusetts Institute of Technology, Cambridge, Massachusetts, USA

Received 29 January 2003; revised 3 February 2004; accepted 30 April 2004; published 23 June 2004.

[1] We apply "residual mean" theory of tracer transport, in which eddy transfer plays a fundamental role, to develop scalings and idealized numerical models of the Southern Ocean uptake of transient tracers. The streamline-averaged numerical model, which represents transport in the meridional plane, captures the observed distributions of CFC-11, bomb-$\Delta^{14}C$, and anthropogenic CO_2. The model reproduces the observed relationship between CFC-11 and bomb-$\Delta^{14}C$ and suggests that the upper branch of the residual overturning flow in the Southern Ocean is about 14 Sv, supporting previous inferences based on the observed buoyancy distribution and air-sea buoyancy fluxes. Scale analysis suggests that the limit of fast air-sea gas exchange is applicable to CFC-11, for which the surface concentration is close to equilibrium and cumulative ocean uptake is largely determined by physical transport processes. In the slow gas exchange limit, applicable to bomb-$\Delta^{14}C$, the surface concentration is far from equilibrium and the cumulative uptake is most sensitive to the parameterization of the gas transfer coefficient. Anthropogenic CO_2 falls between those two limit cases and is sensitive to both transport processes and the gas transfer coefficient. Sensitivity studies using the streamline-averaged model suggest that uncertainties in air-sea buoyancy fluxes in current climatologies result in significant uncertainty in estimates of Southern Ocean uptake of anthropogenic CO_2 based on circulation and biogeochemistry models driven by, or brought into consistency with, the climatological fluxes. This uncertainty is sufficient to explain a significant amount of the spread in a recent model comparison study. *INDEX TERMS:* 4808 Oceanography: Biological and Chemical: Chemical tracers; 4806 Oceanography: Biological and Chemical: Carbon cycling; 4842 Oceanography: Biological and Chemical: Modeling; *KEYWORDS:* residual mean theory, Southern Ocean, transient tracers

Citation: Ito, T., J. Marshall, and M. Follows (2004), What controls the uptake of transient tracers in the Southern Ocean?, *Global Biogeochem. Cycles*, *18*, GB2021, doi:10.1029/2003GB002103.

1. Introduction

[2] Atmospheric CO_2 has been rising rapidly due to anthropogenic emissions, but its rate of increase is mediated by uptake into the oceans and the terrestrial biosphere. Likewise, CFC-11 has rapidly increased in the past several decades from zero to about 260 pptv. Atmospheric $\Delta^{14}C$ peaked in the 1960s due to the nuclear tests (Figure 1). The signature of these tracers has been observed in the global oceans through ship-based measurements during the World Ocean Circulation Experiment (WOCE) and Joint Global Ocean Flux Study (JGOFS), and observations continue. The distributions of these transient tracers have some significant differences reflecting the contrast in their respective input functions (atmospheric trends) and air-sea gas exchange rates. Here we use idealized models to help understand and illustrate the mechanisms that control the distribution and fluxes of these tracers. In turn, tracer observations provide a means to test models of Southern Ocean circulation and quantify the overturning circulation in the region.

[3] The uptake of anthropogenic CO_2 by the Southern Ocean is the subject of intense research. Its distribution has been evaluated using observations of biogeochemical properties and age tracers [*Gruber et al.*, 1996; *Gruber*, 1998; *Sabine et al.*, 1999]. *McNeil et al.* [2003] estimate the anthropogenic CO_2 inventory using its relationship to the CFC age distribution. The rate at which the oceans are absorbing anthropogenic CO_2 is difficult to determine directly from observations because the perturbations are small relative to background, naturally occurring fluxes. Furthermore, ship-based observations are sparse in time and space. For this reason, ocean general circulation and biogeochemical model simulations have been used to provide additional estimates of the distribution and fluxes of anthropogenic CO_2. The Ocean Carbon-cycle Model Inter-comparison Project (OCMIP) examined and compared several general circulation model (GCM) simulations of anthropogenic tracers [*Orr et al.*, 2001; *Dutay et al.*,

0886-6236/04/2003GB002103

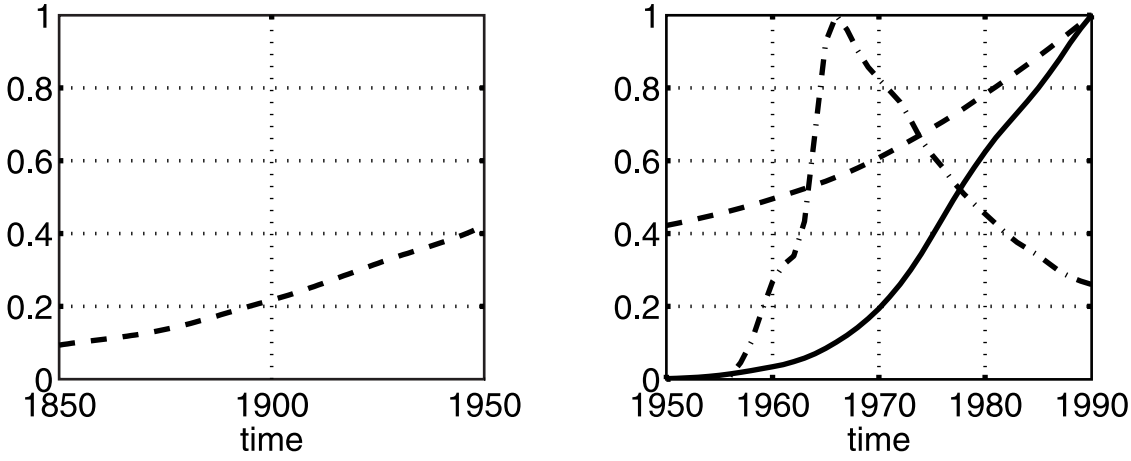

Figure 1. (left) Time history of anthropogenic CO_2 in the atmosphere between 1750 and 1950. (right) Time history of CFC-11, anthropogenic CO_2, and bomb-induced $\Delta^{14}C$ in the atmosphere between 1950 and 1990. The vertical axis is the normalized atmospheric mixing ratio, referenced to the maximum value. Atmospheric CO_2 has the longest history of anthropogenic perturbation.

2002]. *Orr et al.* [2001] show that the Southern Ocean is a major region of ocean uptake of anthropogenic CO_2 in the models, but also find that it is the region where the models show the largest disagreement in air-sea flux.

[4] In the Southern Ocean, baroclinic eddies play a central role in the transport of momentum, buoyancy, and tracers [*Johnson and Bryden*, 1989; *Gille*, 1994; *Karsten et al.*, 2002], and yet they are generally unresolved and crudely parameterized in the large-scale ocean general circulation models. *Robitaille and Weaver* [1995] demonstrated that the choice of subgrid-scale parameterization significantly impact modeled CFC distributions, favoring the *Gent and McWilliams* [1990] (hereinafter referred to as GM90) scheme. *Matear* [2001] showed that the uptake of anthropogenic CO_2 is also sensitive to the numerical schemes and eddy parameterizations employed, particularly in the Southern Ocean. *Caldeira and Duffy* [2000] also demonstrate that isopycnal stirring significantly contributes to the northward transport of anthropogenic CO_2 in the Southern Ocean of an ocean model.

[5] To better understand and interpret the tracer distributions, and the simulations of them, we must closely examine key processes that control the tracer transport and air-sea flux of CO_2 in the region. Surface westerlies drive equatorward Ekman transport which is in part balanced by poleward, eddy-induced transport of properties: The net result is the residual circulation.

[6] Recent studies show that the residual circulation can be diagnosed from surface momentum and buoyancy fluxes [*Marshall*, 1997; *Speer et al.*, 2000; *Karsten and Marshall*, 2002]. These studies employ the Transformed Eulerian Mean [*Andrews and McIntyre*, 1976], which reformulates the tracer transport equation in terms of residual circulation. In this study we examine the transport of anthropogenic tracers in the Southern Ocean using a simple dynamical model of the Antarctic Circumpolar Current (ACC) based on residual mean theory. We consider three transient tracers: CFC-11, anthropogenic CO_2, and bomb-$\Delta^{14}C$. The modeled distributions of CFC-11 and bomb-$\Delta^{14}C$ are compared with observed distributions to evaluate the theoretical interpretations. Sensitivity studies with the model indicate the key factors controlling the distributions of these tracers and their fluxes.

[7] The structure of the paper is as follows. In section 2, we outline a theory of zonally averaged tracer transport in the Southern Ocean. In section 3, we simulate CFC-11 and bomb-$\Delta^{14}C$ distributions and compare with observed distributions. In section 4, we develop a conceptual understanding of the uptake of the transient tracers in some limit cases, and illustrate it with sensitivity experiments. In section 5, we discuss the results and its implications to uncertainty in anthropogenic CO_2 uptake.

2. Physical Transport

[8] The analysis presented here is based on streamline-averaged fields in which velocities and tracer concentrations are averaged along mean streamlines. Figure 2a shows geostrophic streamlines, $\Psi_g = g\overline{h}/f$, in the ACC determined from the 4-year time-averaged, large-scale (2° horizontal resolution) dynamic sea surface height data from TOPEX-Poseidon following *Karsten and Marshall* [2002]. The latitude of the ACC varies with longitude, and is strongly influenced by bottom topography [*Gille*, 1994]. Therefore, taking a simple zonally averaged view (i.e., averaging along latitude circles) obscures the meridional tracer distribution and transport across the meandering jet of the ACC. Hence, hereafter, geostrophic streamlines are assumed to be the meridional coordinate. Figure 2b depicts streamline-averaged potential density as a function of depth (using World Ocean Atlas data [*Levitus and Boyer*, 1994]) showing isopycnals sloping up toward Antarctica.

[9] The significance of using the streamline-averaged framework can be illustrated using tracer observations. Figures 3a through 3f show the distribution of observed

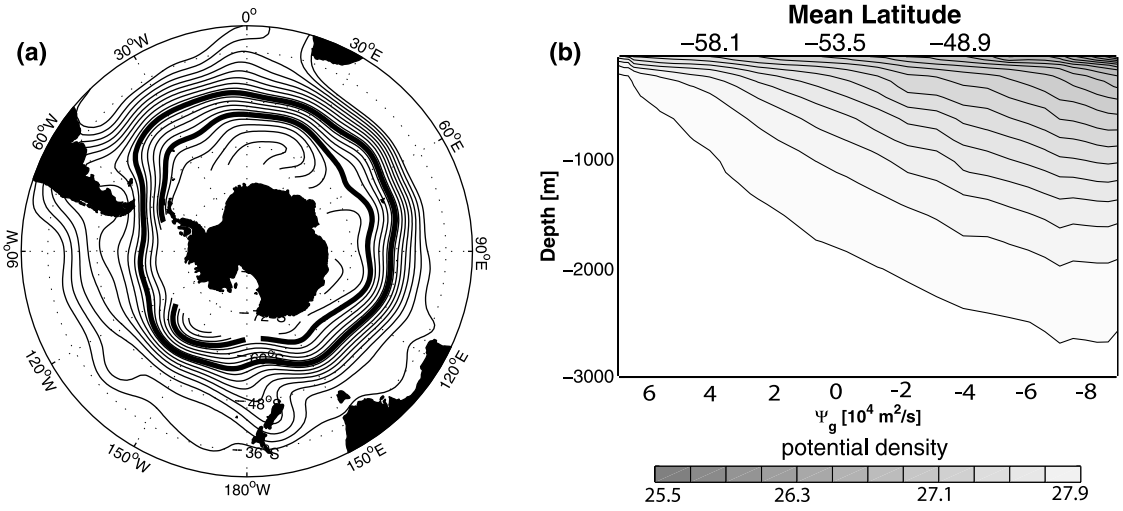

Figure 2. (a) Geostrophic streamlines estimated from a 4-year time average of TOPEX-Poseidon altimetry. The contour interval is 10^3 m^2 s^{-1}. Thick lines indicate approximate positions of the Antarctic Polar Front and the Subantarctic Front. (b) Zonally averaged potential density from *Levitus and Boyer* [1994] climatology.

pCFC-11 in the Atlantic, Indian, and Pacific sector of the ACC. The distribution of pCFC, which is the concentration of CFC-11 normalized by the solubility, is clearly correlated with the structure of the Circumpolar Current. In Figures 3a, 3c, and 3e, pCFC-11 is plotted in latitude-depth coordinates. Here the spatial pattern of pCFC-11 is significantly different between the three sections due to the meandering of the ACC and the fact that the tracer distribution is tightly coupled to the frontal structures. When the same data are plotted in the streamline coordinate, as shown in Figures 3b, 3d, and 3f, the pCFC-11 distribution becomes remarkably similar between the three sections. This correspondence motivates us to use a streamline-averaged tracer transport model since the observed tracer distribution is quasi-two-dimensional in that coordinate system.

2.1. Transport by the "Residual Mean"

[10] We formulate the two-dimensional circulation model following *Karsten and Marshall* [2002] and *Marshall and Radko* [2003] based on residual mean theory [*Andrews and McIntyre*, 1976; *Held and Schneider*, 1999]. We define the streamline averaged concentration, $\overline{C}(y, z)$, hereafter just C, in the streamline coordinate where the y-coordinate is mapped onto the corresponding value of Ψ_g. The zonally averaged prognostic equation for tracers is

$$\frac{\partial C}{\partial t} + v_{res}\frac{\partial C}{\partial y} + w_{res}\frac{\partial C}{\partial z} = \nabla \cdot \mathbf{K}\nabla C - \frac{\partial F}{\partial z}, \qquad (1)$$

where $\mathbf{K}$ is the isopycnal diffusion tensor following *Solomon* [1971]. The air-sea gas flux, F, is parameterized as restoring toward equilibrium with the overlying atmosphere under current physical conditions: $F = -\lambda h(C - C_{at})$. Here λ is the inverse timescale for air-sea gas equilibration, which is linearly related to gas transfer velocity. C_{at} is the saturated concentration in equilibrium with the atmospheric partial pressure. This form can be applied to each of the gases discussed here, with some approximation [*Broecker and Peng*, 1974]. In Table 1 we define the saturated concentrations, C_{at} for each tracer, and detailed definitions of chemical constants can be found in Appendix A. Approximate formulae and values for the air-sea gas exchange timescales of each tracer are given in Table 1.

[11] In equation (1), tracers are advected by the residual mean flow, (v_{res}, w_{res}) in streamline coordinates. It combines the effects of wind-driven and eddy-induced circulation. Figure 4 illustrates, schematically, the dynamical balances in the ACC following *Marshall* [1997]. The Eulerian mean flow, $\overline{\Psi}$, is the Deacon Cell driven by the equatorward directed Ekman flow due to the surface westerly wind. The poleward return flow at depth is assumed to be in geostrophic balance with the zonal pressure gradient supported by bottom topography. $\overline{\Psi}$ is partially compensated by the eddy-induced flow, Ψ_{eddy}, driven by baroclinic eddy transfer. The residual mean flow, Ψ_{res}, is the net transport, the sum of $\overline{\Psi}$ and Ψ_{eddy},

$$\Psi_{res} = \overline{\Psi} + \Psi_{eddy}, \qquad (2)$$

$$\overline{\Psi} = -\frac{\tau_s}{\rho_0 f}, \qquad (3)$$

$$\Psi_{res}|_{-h}\frac{\partial \overline{b}}{\partial y} = \tilde{B}_s. \qquad (4)$$

Here $\overline{\Psi}$ is the Ekman transport set by the surface wind stress forcing, τ_s, as in equation (3). We diagnose the residual circulation, Ψ_{res}, from the surface buoyancy forcing following *Marshall* [1997]: The residual stream function at the base of surface mixed layer, $\Psi_{res}|_{-h}$, is determined by the steady state buoyancy balance. In equation (4), the

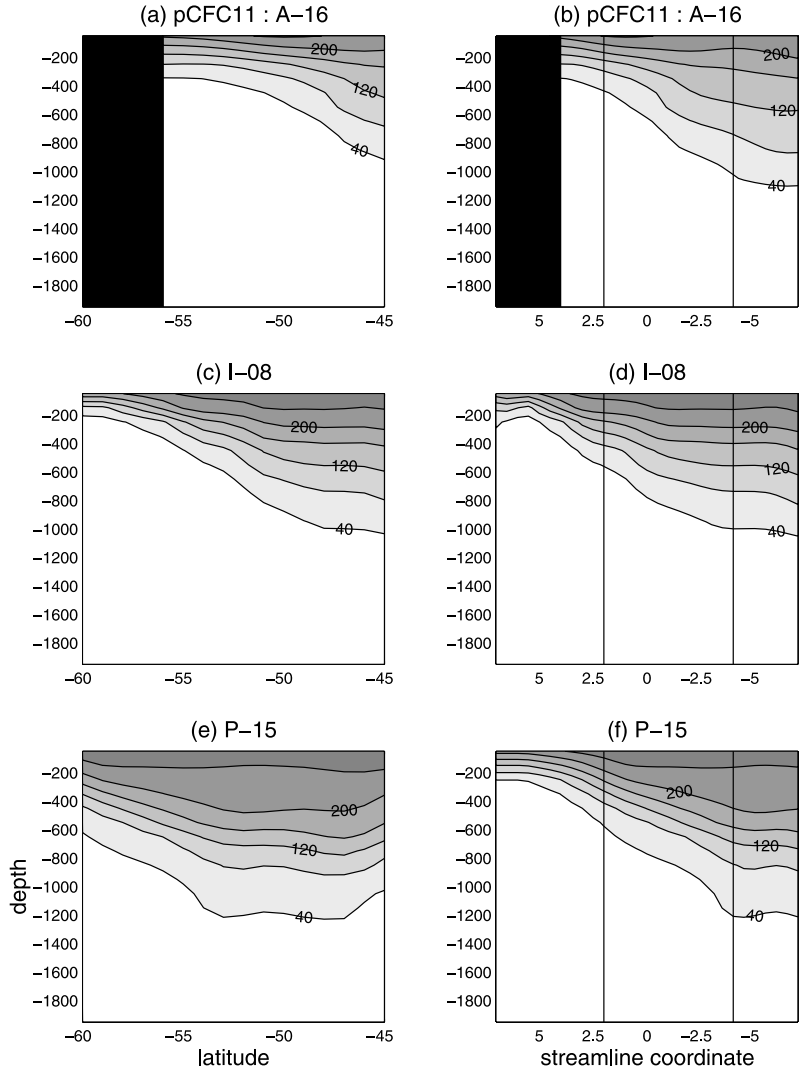

Figure 3. Observed pCFC-11 distribution from three WOCE sections in units of pptv. Data in the left column are plotted in latitude-depth coordinates. Figures in the right column are in the streamline-depth coordinates. Data are shown from WOCE lines in the (a, b) Atlantic, A-16, (c, d) Indian Ocean, I-08, and (e. f) Pacific, P-15. The units for streamlines are 10^4 m^2 s^{-1} in Figures 3b, 3d, and 3f. The two vertical lines in Figures 3b, 3d, and 3f mark the position of the Polar Front and the Subantarctic Front (Figure 2).

surface buoyancy fluxes and the diapycnal eddy fluxes are combined into diabatic flux, $\tilde{B}_s = B_s - \int_{-h}^{0} \frac{\partial}{\partial y} \overline{v'b'} dz$, [*Marshall*, 1997; *Marshall and Radko*, 2003] where B_s is the air-sea buoyancy flux, the combined effect of heat and freshwater exchanges. Thus Ψ_{res} and $\overline{\Psi}$ can, in principle, be diagnosed from surface wind stress and buoyancy forcing.

[12] *Marshall and Radko* [2003] present simple solutions for the ACC and its overturning stream function based on equations (2)–(4). Ψ_{eddy} is parameterized, following GM90, as proportional to the isopycnal slope, s_ρ. In addition, following *Visbeck et al.* [1997] (hereinafter referred to as V97), the eddy transfer coefficient is also set proportional to s_ρ. Thus

$$K = k|s_\rho|, \tag{5}$$

Table 1. Simple Formulae for Saturated Concentrations and Air-Sea Gas Exchange Rates of CFC-11, Anthropogenic CO_2, and Bomb-$\Delta^{14}C$[a]

	CFC − 11	CO_2	$\Delta^{14}C$
C_{at}	$k_{\mathrm{CFC-11}} p\mathrm{CFC}$	$\frac{\mathrm{DIC}_0}{p\mathrm{CO}_{20} Bu}(p\mathrm{CO}_2 - p\mathrm{CO}_{20})$	$\Delta^{14}C_{atm}$
λ	$\frac{K_w}{h}$	$\frac{K_w p\mathrm{CO}_{20}\mathrm{Bu}}{h\mathrm{DIC}_0}$	$\frac{K_w p\mathrm{CO}_{20}}{h\mathrm{DIC}_0}$
$O(1/\lambda)$	0.1 (year)	1 (year)	10 (years)

[a]Here $k_{\mathrm{CFC-11}}$ is the solubility of CFC-11, K_w is the gas transfer coefficient, and Bu is the Buffer factor. We parameterize the gas transfer coefficient, K_W, following *Wanninkhof* [1992] with idealized profiles of temperature, salinity, and surface wind. DIC_0 and $p\mathrm{CO}_{20}$ are preindustrial distribution of DIC and $p\mathrm{CO}_2$. Detailed derivations are presented in Appendix A.

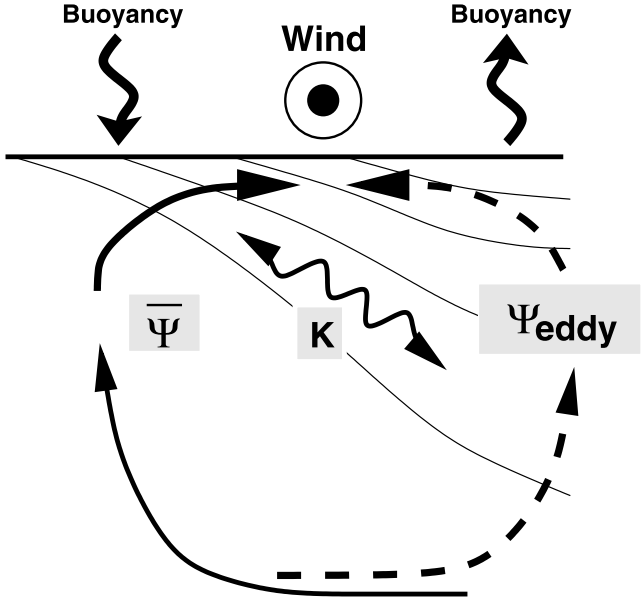

Figure 4. A schematic diagram illustrating the dynamical balance in the ACC. Wind-driven, Eulerian mean flow and eddy-induced flow are shown as solid and dashed lines, respectively. They can be inferred from the surface physical forcing (wind stress and buoyancy fluxes) and surface buoyancy distribution [after *Marshall*, 1997].

where k is a coefficient of eddy closure. The eddy-induced stream function is thus parameterized as

$$\Psi_{eddy} = -k s_\rho{}^2. \tag{6}$$

[13] Using equations (2)–(6) the isopycnal slope can be expressed in terms of patterns of external physical forcing,

$$|s_\rho| = \sqrt{-\frac{\tau_s}{k f \rho_0} - \tilde{B}_s \left(k \frac{\partial \overline{b}}{\partial y} \right)^{-1}}. \tag{7}$$

Note the simple, square-root relationship between surface wind stress and isopycnal slope, a consequence of the choice of eddy parameterization following V97.

[14] The method of characteristics allows one to map a prescribed surface buoyancy distribution down into the interior. We calculate the depth of each isopycnal layer by horizontal integration of the slope of the isopycnal as it dips down into the thermocline. We assume that diapycnal mixing is negligible in the ocean interior, allowing us to set the residual stream function, Ψ_{res}, to be constant on each isopycnal surface. We integrate from the base of the surface mixed layer where equation (4) sets the boundary condition for Ψ_{res}, and the isopycnal slope is calculated by equation (7). Here we set the mixed layer depth to a constant, h = 200 m, and the eddy closure parameter, $k = 1 \cdot 10^6$ m^2 s^{-1} as per *Marshall and Radko* [2003].

2.2. Forcing Functions and Solutions

[15] Figure 5 shows the streamline-averaged thermal component of the analyzed surface buoyancy flux from several climatologies including the National Centers for Environmental Prediction-National Center for Atmospheric Research (NCEP-NCAR) reanalysis [*Kalnay et al.*, 1996],

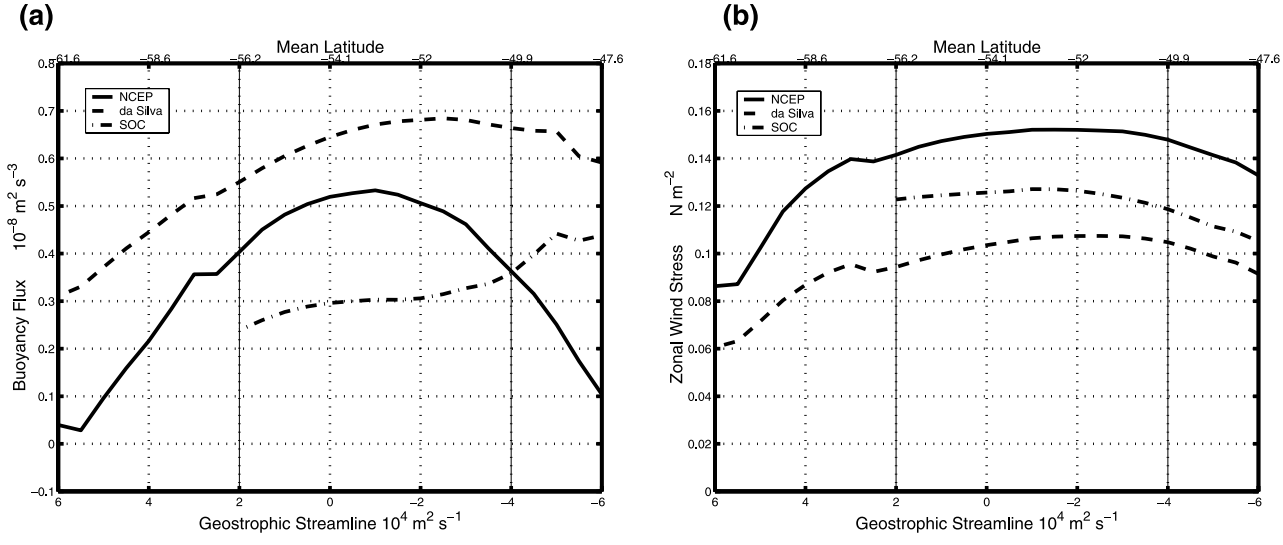

Figure 5. Streamline averaged surface fluxes from NCEP-NCAR reanalysis data, the *da Silva et al.* [1994] data set, and the SOC data set. (a) Heat flux contribution to air-sea buoyancy flux in units of m^{-2} s^{-3}. (b) Surface wind stress in units of N m^{-2}. The data are plotted in the streamline coordinate, and the two vertical lines mark the position of the Polar Front and the Subantarctic Front.

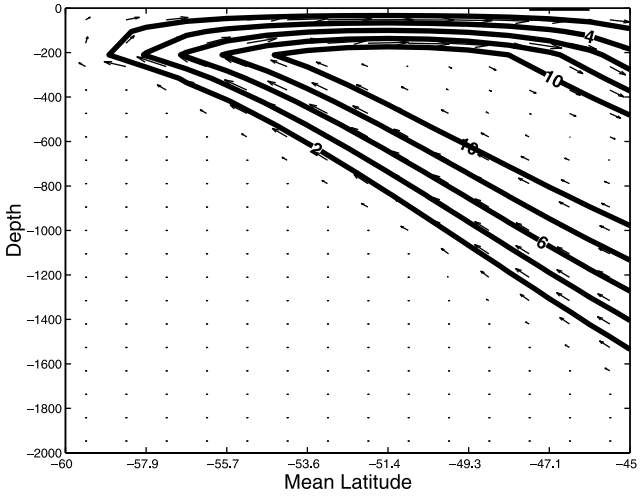

Figure 6. Residual stream function (Sv) determined from the idealized surface wind stress and buoyancy flux distributions using the method of characteristics, following *Marshall and Radko* [2003].

da Silva Surface Marine Data [*da Silva et al.*, 1994], and the SOC climatology [*Josey et al.*, 1999]. These data sets are not in quantitative agreement in the Southern Ocean, but they show a common qualitative structure with a positive buoyancy input into the mixed layer to the south of the ACC. From equation (4), this is suggestive of equatorward residual advection at the surface. There is a decrease in air-sea buoyancy flux to the north of the ACC implying subduction of water masses there [*Marshall*, 1997; *Karsten and Marshall*, 2002]. The large differences in amplitude of the buoyancy flux climatologies will manifest themselves as large uncertainties in the intensity of the residual flow estimates based on them. In this paper, for simplicity, we use surface heat flux and surface temperature as a measure of buoyancy forcing. The freshwater component of the air-sea buoyancy flux is even more uncertain and is not used in this analysis. In contrast, the wind stress forcing seems more consistent between climatologies (Figure 5).

[16] On the basis of the climatologies in Figure 5, we construct an idealized profile of surface buoyancy and wind-forcing, approximately an average of the three data sets. Applying equations (2)–(7), we calculate the interior buoyancy distributions, residual circulation, and isopycnal eddy diffusivity as outlined in the previous section. In the solution (Figure 6), Circumpolar Deep Water (CDW) upwells to the south of the ACC, moves equatorward at the surface, and subducts into the thermocline near the polar front, forming Antarctic Intermediate Water (AAIW). The maximum Ψ_{eddy} is about 14 Sv, and the pattern of residual flow is broadly similar to the circulation estimated by *Karsten and Marshall* [2002], who diagnose eddy fluxes directly from satellite sea surface height data. The implied isopycnal eddy transfer coefficient in this solution has a peak value of 1250 $m^2\ s^{-1}$ to the north of the ACC and decreases away from it. The particular choice of k modulates the isopycnal slope, s_ρ, and the isopycnal eddy diffusivity, K. Note that our model extends to approximately 60°S and does not explicitly represent the formation of Antarctic Bottom Water (AABW).

[17] Baroclinic eddies have a large impact on the resulting tracer distributions through both advective and diffusive (stirring) influences. The eddy-induced flow in equation (6) represents the advective component of baroclinic eddy transfer shown in Figure 6. Isopycnal stirring in equation (1) is the diffusive component of the same dynamical process. Both are represented in the tracer model based on equation (1).

3. What Controls the Distribution of Transient Tracers?

[18] We have developed a numerical model which integrates the tracer equation (1), based on the residual mean circulation determined as described in the previous section and illustrated in Figure 6. The model has a horizontal resolution of 1° and 15 vertical levels from the surface to 3000 m, and advective transport is discretized using a second-order finite difference scheme. The tracer model is integrated from 1765 to 1990 for anthropogenic CO_2, CFC-11, and bomb-$\Delta^{14}C$, forced by the atmospheric transients depicted in Figure 1. The air-sea gas transfer coefficient, K_W, is a function of the wind speed according to *Wanninkhof* [1992].

[19] Figures 7a and 7b show the modeled distributions of CFC-11 and associated pCFC-11 in 1994. The corresponding observations from the WOCE Indian section, I-08, along ~90°E, are shown in Figures 7c and 7d. Similarly, Figures 8a and 8b, respectively, show modeled and observed (I08) distributions of bomb-$\Delta^{14}C$. The observed distribution is determined using the potential alkalinity method of *Rubin and Key* [2002].

[20] Comparison of modeled and observed fields must be carried out with caution because the modeled fields are streamline-averaged whereas the observations are from a particular section. However, examination of several WOCE sections across the ACC in streamline coordinates reveals rather similar distributions of CFC-11 (Figures 3b, 3d, and 3f), suggesting that qualitative comparison of the model and observations may be useful.

[21] We find a reasonable agreement between the modeled and observed distributions of CFC-11 and bomb-$\Delta^{14}C$. The magnitude of the tracer concentrations and their large-scale gradients are captured by the zonally averaged model. The modeled CFC-11 and bomb-$\Delta^{14}C$ distributions have slightly shallow penetration depths compared to the observations. This is because tracer transport is essentially isopycnal in the interior and the modeled isopycnals are slightly too shallow. At the surface, CFC-11 is close to saturation, and its meridional gradient reflects the variation of the solubility, which is largely controlled by sea surface temperature (SST). Hence pCFC-11 does not exhibit a surface gradient. Surface bomb-$\Delta^{14}C$ is slightly overestimated compared to that diagnosed from the WOCE I-08 section.

[22] We also evaluate the modeled distributions in terms of the relationships between CFC-11 and bomb-$\Delta^{14}C$

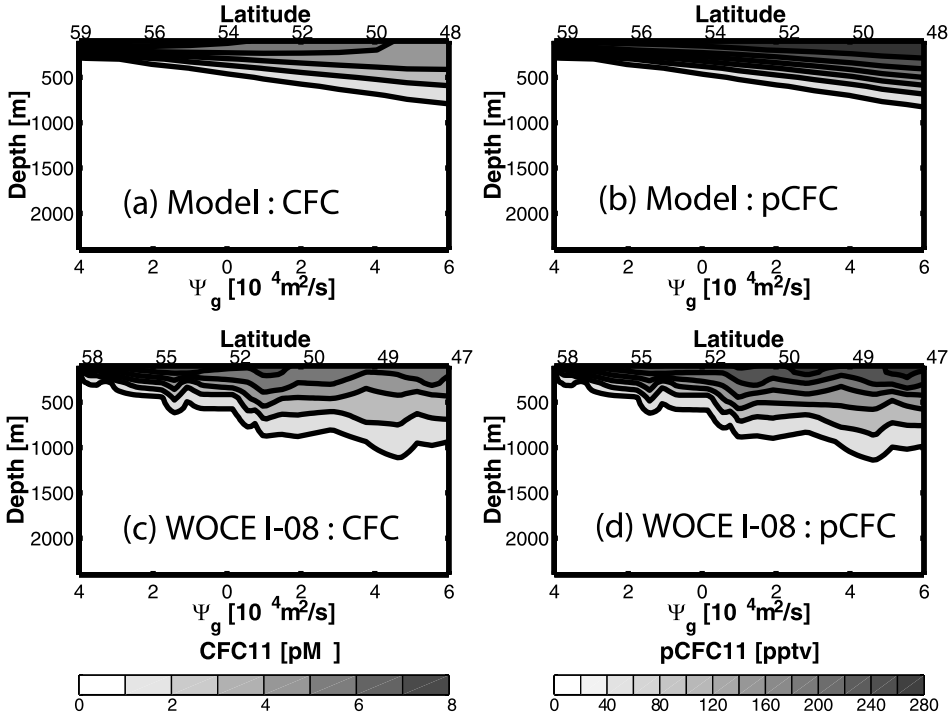

Figure 7. (a, b) Simulated 1994 distribution of CFC-11 and pCFC-11 and (c, d) observed CFC-11 and pCFC-11 from WOCE Indian section, I-08.

(Figure 9). The observed sections show two modes of correlation between the tracers. Figure 9 shows a positive correlation in the thermocline and a negative correlation in the surface layer along the WOCE I-08 line. This pattern of tracer relationship is common to all the available sections in the ACC. What processes control this pattern of correlations and do the modeled tracers reflect it?

[23] Our simple model can indeed reproduce the general patterns of observed correlation between CFC-11 and bomb-Δ^{14}C and shows that the residual circulation plays an important role in controlling the correlation at the surface. The meridional gradients of CFC-11 and bomb-Δ^{14}C are of opposite sign in the surface layer. This is because CFC-11 and bomb-Δ^{14}C have very different air-sea equilibration timescales, λ [*Broecker and Peng*, 1974], and different spatial variations in solubility.

[24] CFC-11 has a monthly timescale for air-sea equilibration, $O(\lambda_{CFC-11}) = 10^{-7}$ s^{-1} (see Table 1), and its solubility increases poleward due to temperature dependence. Figure 10 schematically illustrates the large-scale distribution and controls on CFC-11 in the 1990s. We may assume a fast gas-exchange limit for CFC-11 such that surface waters are very close to equilibrium. The concentration decreases along isopycnals, reflecting the surface source and increasing atmospheric mixing ratio.

[25] In contrast, bomb-Δ^{14}C has a decadal timescale for air-sea exchange, $O(\lambda_{\Delta^{14}C}) = 10^{-9}$ s^{-1}, and decreases poleward in the surface Southern Ocean because upwelling of uncontaminated waters are advected equatorward more rapidly than they can accumulate bomb-Δ^{14}C from the atmosphere. Figure 11 schematically depicts the controls on bomb-Δ^{14}C. We assume a limit for bomb-Δ^{14}C in which the air-sea gas exchange is much slower than the physical transport and surface waters may be far from solubility equilibrium: $C \ll C_{at}$. To the south of the polar front, where deep water upwells, the surface bomb-Δ^{14}C concentration is determined by a competition between air-sea flux and upwelling. An equatorward advection and accumulation of bomb-Δ^{14}C is consistent with positive buoyancy fluxes into the ocean shown in Figure 5.

[26] The signs of isopycnal gradients of CFC-11 and bomb-Δ^{14}C are the same in the thermocline because the only source of these tracers is from the atmosphere. Anthropogenic CO_2, to be discussed in more detail later, falls between these two tracers, with an equilibration timescale on the order of 1 year (Table 1).

[27] Since the residual circulation has a significant control on the surface bomb-Δ^{14}C distribution, but not on that of CFC-11, their relative distributions provide a clear, qualitative measure of the residual flow. The streamline-averaged model successfully captures the relative distributions between CFC-11 and bomb-Δ^{14}C and helps to illustrate the controlling mechanisms.

[28] We can use tracer-tracer relationships to examine more complex, three-dimensional general circulation and biogeochemistry models. In particular, the correlation of the surface CFC-11 and bomb-Δ^{14}C provides a point of comparison with observations. Figure 12 shows the relationship between CFC-11 and bomb-Δ^{14}C in a coarse-resolution three-dimensional configuration of the MITgcm [*Marshall et al.*, 1997a, 1997b] used for tracer simulations in OCMIP [e.g., *Dutay et al.*, 2002]. This particular configuration parameterizes subgrid-scale eddy transfers using GM90 and isopycnic eddy stirring with a uniform diffusivity.

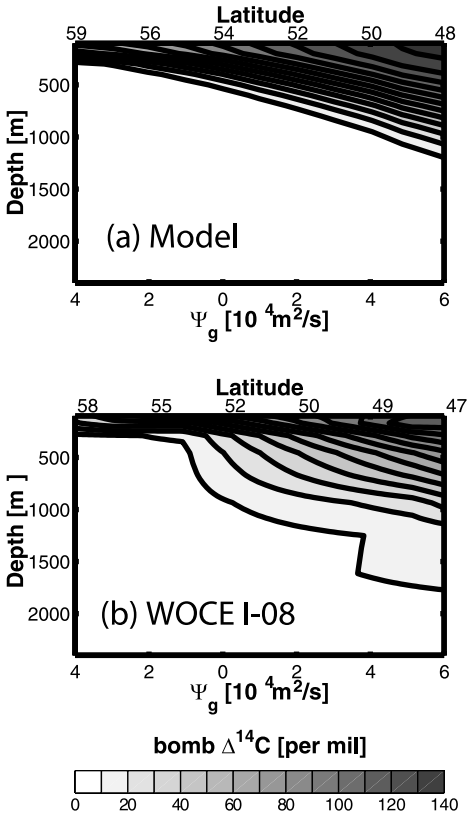

Figure 8. (a) Simulated and (b) observed distribution of bomb-Δ^{14}C in 1994 along WOCE Indian section (I-08). Bomb-Δ^{14}C distributions are diagnosed from observed Δ^{14}C using the potential alkalinity method of *Rubin and Key* [2002].

The model is forced with seasonally varying wind stress and buoyancy forcing. Comparing Figures 12 and 9 shows that this particular model set-up does not capture the sharp contrast in surface and thermocline gradients seen in the data and the streamline-averaged model. This is because the simulated residual overturning circulation is very weak in the Southern Ocean of this simulation (Figure 13). The wind-driven and eddy-induced transport almost cancel one another out, and the thermocline in the model's ACC is mainly ventilated by isopycnal eddy stirring.

4. What Controls the Uptake of the Transient Tracers?

[29] In the previous section we discussed the controls on the distribution of transient tracers in the Southern Ocean. In this section we consider the controls on the air-sea tracer flux using scaling arguments and sensitivity experiments with the streamline-averaged model. How are the large-scale patterns of uptake of CFC-11, bomb-Δ^{14}C, and anthropogenic CO_2 controlled in the model? What is the rate-limiting process in the uptake of these tracers? How are these fluxes affected by changes in the physical forcing?

[30] We first examine the time-averaged tracer balance in the surface layer. We integrate the tracer equation (1), over the depth of the mixed layer and estimate the relative magnitude (s^{-1}) of each term,

$$\frac{\partial C}{\partial t} + v_{res}\frac{\partial C}{\partial y} + \frac{\bigwedge w_{res}|_{-h}}{h}(C - C_{th}) = -\frac{Ks_\rho}{h}\left(\frac{\partial C}{\partial y}\right)_{\rho,-h} + \frac{\partial}{\partial y}K\frac{\partial C}{\partial y} - \lambda C + \lambda C_{at}. \quad (8)$$

Scaling and magnitude are given in Table 2. The third term on the left-hand side represents entrainment and is only

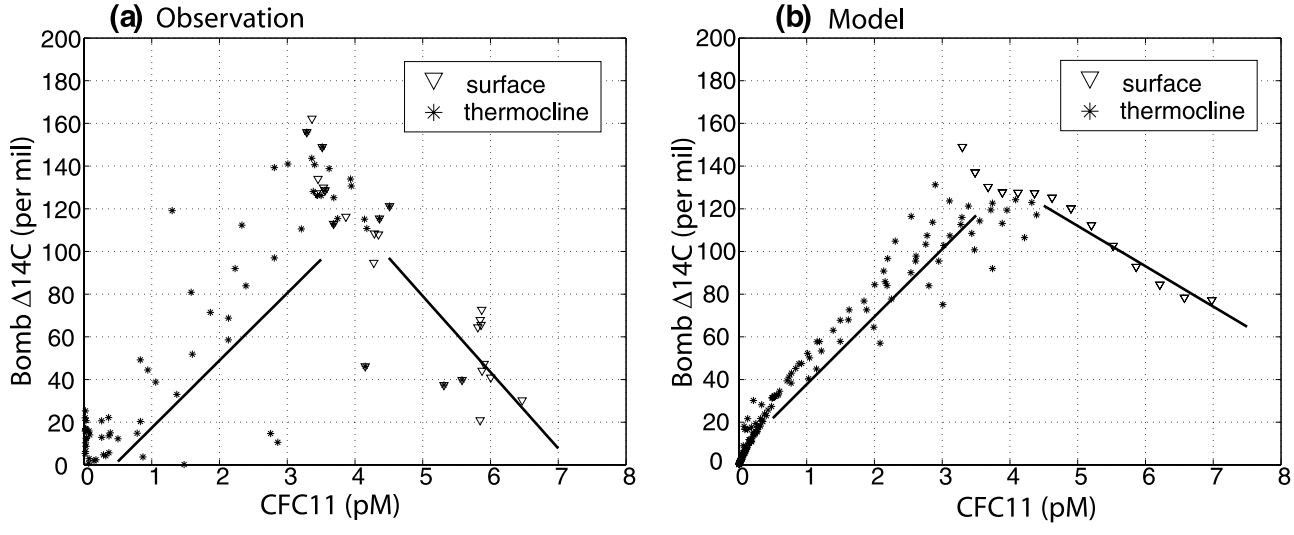

Figure 9. Scatterplot of CFC-11 versus bomb-Δ^{14}C in the Southern Ocean to the south of 45°S. (a) Observations from WOCE line I-08, and (b) model. Solid lines indicate least squares fits to the data above and below 200 m. In the surface layer, CFC-11 and bomb-Δ^{14}C distributions are negatively correlated. Below the surface layer, the correlation becomes positive. The streamline-averaged model captures the pattern of the observed relationship.

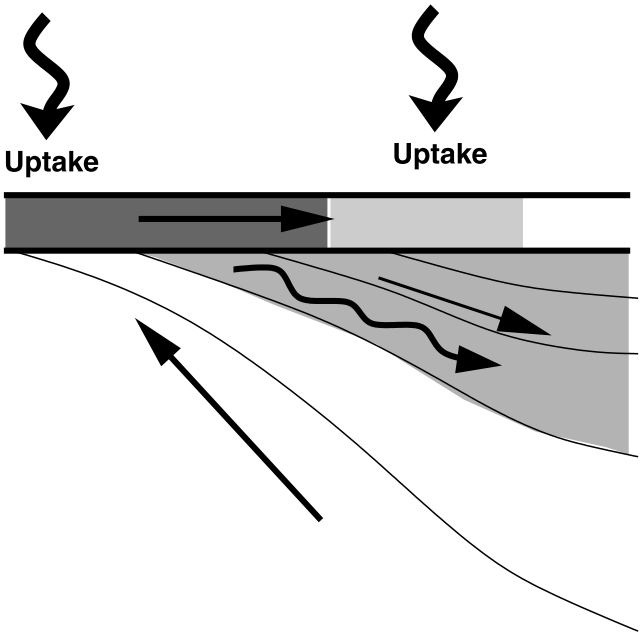

Figure 10. Schematic diagram of the uptake of CFC-11. Large-scale upwelling drives strong uptake of CFC-11 to the south of the ACC and isopycnal stirring drives another peak the uptake to the north of the ACC. In between, there is a region of minimum uptake due to the equatorward advection and warming of surface waters.

active when the water is upwelling: $\wedge$ is 1 when w_{res} is positive, and is 0 otherwise. C_{th} represents the tracer concentration in the upper thermocline. The first term on the right-hand side is due to isopycnal stirring at the base of the mixed layer, and $(\partial C/\partial y)_{\rho,-h}$ represents the isopycnal tracer gradient just below the mixed layer. The second term on the right-hand side is the divergence of horizontal, diapycnal eddy fluxes assuming that eddy transfer is directed horizontally in the mixed layer. We are interested in interannual to decadal timescales, and it is appropriate to assume that local accumulation in the mixed layer is negligible compared to physical transport.

[31] The relative magnitudes of the terms in equation (8) are estimated using the following parameter values: The magnitude of the residual circulation can be estimated from equation (4), $\Psi_{res} \sim B_s L \Delta b^{-1}$. For a buoyancy change across the ACC, $\Delta b = 7 \cdot 10^{-3}$ m s^{-2}, a surface buoyancy flux, $B_s = 5 \cdot 10^{-9}$ m^2 s^{-3} and the meridional scale of ACC, $L = 10^6$ m, we find $O(\Psi_{res}) = 0.7$ m^2 s^{-1}. We also assume a thickness of the surface mixed layer, $O(h) = 10^2$ m, and a thermocline depth, $O(H) = 10^3$ m. The gross magnitude of isopycnal eddy diffusivity is $O(K) = 10^3$ m^2 s^{-1}. Combining these parameters, we arrive at our estimates of the surface transport terms shown in equation (8). We see that the residual flow and isopycnal stirring are of comparable magnitude, but diapycnal eddy fluxes are an order of magnitude smaller than other terms.

4.1. CFC-11

[32] Figure 14 shows the cumulative uptake of CFC-11 in the streamline-averaged model and its sensitivity to buoyancy fluxes (represented by Ψ_{res}), wind stress (represented by $\overline{\Psi}$), and gas transfer coefficient. We define the cumulative air-sea fluxes, $FT(y, t)$, thus

$$FT(y) = \int_{t_0}^{t_1} \lambda h \, (C_{at} - C) \, dt, \tag{9}$$

where $t_0 = 1750$ is the initial time of the model integration and $t_1 = 1990$ is the end time.

[33] In each panel of Figure 14, solid lines represent the control run which are carried out with the standard set of physical parameters. In the sensitivity runs, depicted by dashed lines, parameters are varied while the spatial patterns are kept fixed. Thus we only examine sensitivities to the magnitude of the physical forcing, not its spatial structure.

[34] The cumulative uptake of CFC-11 exhibits two peaks in the control run at around 60°S and 48°S. What controls the spatial patterns of the uptake? In short, the larger peak to the south of the ACC is due to upwelling of cold, deep water and higher solubility. The secondary peak to the north of the ACC is due to enhanced isopycnal stirring. Using simple theory and scaling analysis, we will illustrate which processes dominate the spatial patterns and magnitude of the cumulative uptake.

[35] We consider the tracer balance in the surface layer shown in equation (8). We assume a fast gas exchange limit for CFC-11 which has a short air-sea equilibration timescale (order 1 month) relative to the timescales of physical

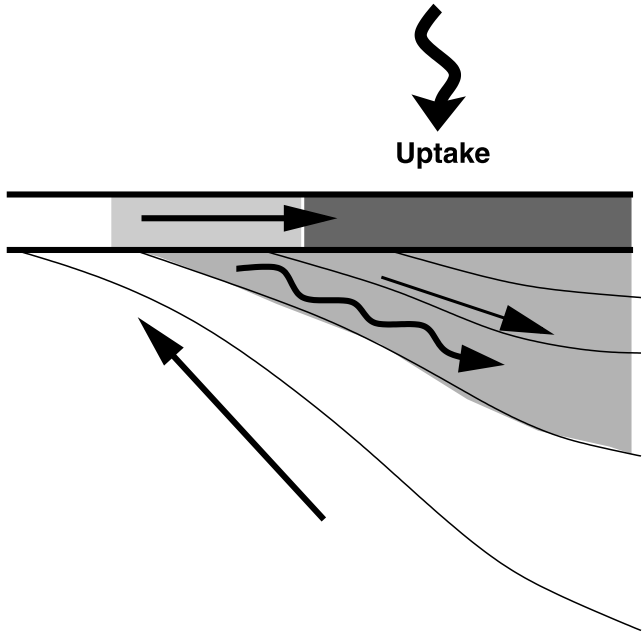

Figure 11. Schematic diagram of the uptake of bomb-Δ^{14}C. The gas transfer coefficient controls the uptake. The maximum uptake occurs where the surface wind speed is strongest. In contrast, the surface distribution of bomb-Δ^{14}C reflects the large-scale circulation with an equatorward surface gradient caused by the accumulation of bomb-Δ^{14}C in the equatorward residual flow.

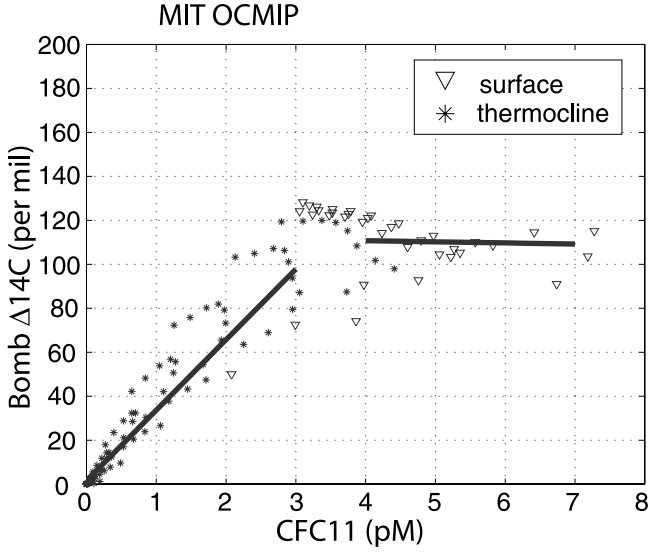

Figure 12. Scatter diagram of CFC-11 and bomb-Δ^{14}C in the Southern Ocean to the south of 45°S calculated in the coarse-resolution configuration of the MIT ocean model used in the OCMIP study [e.g., *Dutay et al.*, 2002]. The plotted model results are from the longitude of WOCE line I-08 in the Indian Ocean. Compare Figure 9a; this particular model configuration does not capture the negative correlation in the surface waters.

transport. Adopting this value for λ in equation (8), we find the leading order balance is dominated by air-sea gas exchange. Hence

$$C \sim C_{at}, \tag{10}$$

and so the surface distribution of CFC-11 is controlled by atmospheric pCFC-11 and the temperature dependent solubility.

[36] At the next order (i.e., retaining the next order of terms in the balance) we find that the small deviation from equilibrium, $\Delta C \equiv C - C_{at}$, is controlled by the physical transport,

$$\Delta C = -\frac{1}{\lambda}\left[v_{res}\frac{\partial C_{at}}{\partial y} + \frac{\bigwedge w_{res}|_{-h}}{h}(C_{at} - C_{th}) + \frac{Ks_\rho}{h}\left(\frac{\partial C_{at}}{\partial y}\right)_{\rho,-h}\right]. \tag{11}$$

The air-sea gas exchange, $F = -\lambda h \Delta C$, is now controlled by physical transport, residual flow, and isopycnal stirring. Note that in this fast exchange limit, the uptake of CFC-11 becomes insensitive to the gas transfer coefficient.

[37] We now consider three idealized cases in which the air-sea gas exchange is balanced by a combination of the three processes in equation (11): (1) entrainment of thermocline waters, (2) horizontal advection, and (3) isopycnal stirring.

4.1.1. Entrainment

[38] Consider a balance between entrainment and air-sea fluxes, a regime that is relevant to the south of the ACC (around 58°S), where there is large-scale upwelling in the residual flow and entrainment of deep waters. Assuming that the upwelling waters are depleted in transient tracers ($C_{th} \ll C_{at}$), we obtain a simple expression for the local uptake,

$$F \sim \frac{w_{res}|_{-h}}{h} C_{at} = \frac{\partial \Psi_{res}}{\partial y}\frac{C_{at}}{h}. \tag{12}$$

The uptake depends on the upwelling rate of the residual circulation, which is also linearly related to the meridional gradient of the surface buoyancy forcing; see equation (4). Thus the uptake rate is related to the surface buoyancy flux in this region. Figure 14 shows the meridional distribution of the cumulative uptake of CFC-11 from the streamline-average numerical model. Each of the three panels depicts the result from the control run (solid line) and two sensitivity studies relating to changes in (Figure 14a)

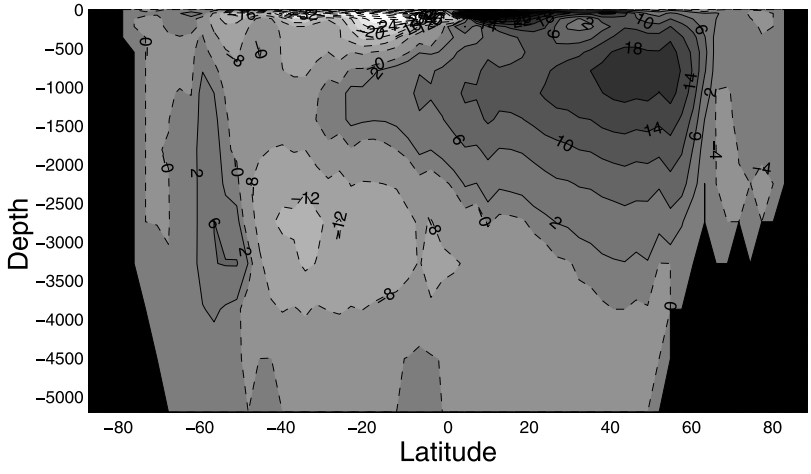

Figure 13. Simulated residual mean overturning circulation, Ψ_{res} (Sv), from the coarse-resolution OCMIP configuration of the MIT ocean model. Note the weak residual overturning in the Southern Ocean: In this configuration the Eulerian mean flow and eddy advection almost exactly cancel.

Table 2. Scaling and Magnitudes for Terms in Equation (8)

	$\frac{\partial C}{\partial t}$	$v_{res}\frac{\partial C}{\partial y}$	$\frac{\Delta w_{res}\vert_{-h}}{h}(C - C_{th})$	$-\frac{Ks_\rho}{h}(\frac{\partial C}{\partial y})_{\rho,-h}$	$\frac{\partial}{\partial y}K\frac{\partial C}{\partial y}$	λC	λC_{at}
Scaling	$O(\frac{C}{T})$	$O(\frac{\Psi_{res}C}{hL})$	$O(\frac{\Psi_{res}C}{hL})$	$O(\frac{KHC}{hL^2})$	$O(\frac{KC}{L^2})$	$O(\lambda C)$	$O(\lambda C^{at})$
Magnitudes	10^{-9}	10^{-8}	10^{-8}	10^{-8}	10^{-9}	λ	$\lambda\frac{C^{at}}{C}$

Ψ_{res}, the residual flow, here related to buoyancy forcing, (Figure 14b) $\overline{\Psi}$, the wind-driven circulation (Deacon Cell), and (Figure 14c) K_W, the gas transfer coefficient. Figure 14a illustrates that the spatial pattern of cumulative uptake is very sensitive to Ψ_{res} and hence to the pattern of buoyancy forcing. The uptake to the south of the ACC is reduced with weaker residual flow because upwelling of deep water is reduced, and consistent with the scaling in equation (12).

4.1.2. Horizontal Advection

[39] Near the polar front (around 53°S), Figure 6 shows a maximum in the equatorward, surface residual flow. Here the horizontal advection in the mixed layer could play an important role in controlling uptake. Assuming a local balance between uptake and horizontal advection by the residual flow, we have

$$F \sim v_{res}\frac{\partial C_{at}}{\partial y} = \frac{\Psi_{res}}{h}\frac{\partial C_{at}}{\partial y}. \tag{13}$$

Depending on the direction of the flow, meridional advection might supersaturate or undersaturate the surface concentration. This parameterization of the surface flux is analogous to the potential solubility model of *Keeling et al.* [1993] and *Murnane et al.* [1999]. The sign of $(\partial C_{at}/\partial y)$ is negative in the ACC due to the equatorward increase in SST. The residual stream function, Ψ_{res}, is positive (i.e., northward) here, and so equation (13) suggests local outgassing in the equatorward residual flow: Cold, CFC-11-rich water is advected and warmed, moving toward supersaturation, and the ocean uptake is small.

[40] The sensitivity experiment shown in Figure 14a reveals that the uptake of CFC-11 near the polar front, around 53°S, is highly sensitive to the variations in Ψ_{res}, which is linearly related to surface buoyancy flux. Hence a 50% decrease in the residual flow causes a comparable increase in the local uptake, consistent with the linear relationship predicted by equations (12) and (13).

[41] We note that the observed climatological distribution of buoyancy flux has significant uncertainty (>50%, see Figure 5) illustrated by the difference between the climatologies. This implies a comparable uncertainty in the regional patterns of air-sea flux of CFC-11 determined with any model forced by these physical data sets.

4.1.3. Isopycnic Stirring

[42] To the north of the ACC, the surface wind is intense and surface buoyancy fluxes suggest that the residual flow is weak. Here it is likely that isopycnic stirring dominates the physical transport. For this regime, we may assume a local balance between isopycnal stirring and air-sea flux of CFC-11.

$$F \sim \frac{Ks_\rho}{h}\left(\frac{\partial C_{at}}{\partial y}\right)_{\rho,-h} = \frac{\Psi_{eddy}}{h}\left(\frac{\partial C_{at}}{\partial y}\right)_{\rho,-h}. \tag{14}$$

Here isopycnal stirring depends on the product of isopycnal diffusivity, isopycnal slope, and tracer gradient at the base of the mixed layer. In this regime, equation (14) suggests that uptake is linearly related to the eddy-induced circulation, Ψ_{eddy}, which depends on surface wind stress, surface buoyancy fluxes, and the specific choice of eddy transfer parameterization. From equations (2)–(6), the eddy-induced transport is $\Psi_{eddy} = \Psi_{res} - \overline{\Psi}$. Note that Ψ_{eddy} and $\overline{\Psi}$ tend to cancel out one another. Thus the magnitude of Ψ_{eddy} and the diffusive flux increases with stronger wind and greater $\overline{\Psi}$. Equation (14) also predicts that the uptake associated with the diffusive fluxes decreases with Ψ_{res} (which reflects buoyancy forcing). This prediction is supported by sensitivity studies with the numerical model shown in Figures 14a and 14b.

[43] In summary, in the control run of the numerical model (Figure 14a, solid line) we find two major regions of uptake of CFC-11 in the Southern Ocean. The first is to the south of the ACC, due to large-scale upwelling and high solubility; the second is due to the intensified isopycnal stirring to the north of the polar front. The region of minimum uptake in between is due to equatorward residual flow. These regimes are schematically illustrated in Figure 10. The sensitivity of uptake in these regimes is also consistent with the idealized scalings derived from equations (10) and (11) in the fast gas exchange limit.

4.2. Bomb Δ^{14}C

[44] Figure 15 shows the streamline-averaged, cumulative uptake of bomb-Δ^{14}C and its sensitivity to buoyancy fluxes (Ψ_{res}), wind stress ($\overline{\Psi}$), and gas transfer coefficient. The cumulative flux is defined in equation (9). The numerical model suggests that uptake of bomb-Δ^{14}C is only sensitive to the gas transfer coefficient (Figure 15c) and the spatial pattern of the uptake reflects that of K_w.

[45] For bomb-Δ^{14}C, the air-sea gas exchange is much slower than the physical transport. In this limit, surface water may be far from the solubility equilibrium, $C \ll C_{at}$. Then the leading order balance in equation (8) is

$$F = \lambda h C_{at}. \tag{15}$$

This approximation has its limitations in the subtropics where the surface concentration approaches C_{at} in the 1990s; the significance of this assumption can be seen in the numerical experiments. Since we assume that atmospheric concentration is spatially uniform, spatial patterns of the uptake are controlled by the profile of gas transfer coefficient, K_w, which, in the numerical experiments, is a function of wind speed following *Wanninkhof* [1992].

[46] Figure 15 shows that variations in Ψ_{res} (buoyancy forcing) and $\overline{\Psi}$ (wind stress forcing) have relatively small impact on the uptake, even though the large-scale distribution of bomb-Δ^{14}C is very sensitive to the surface residual

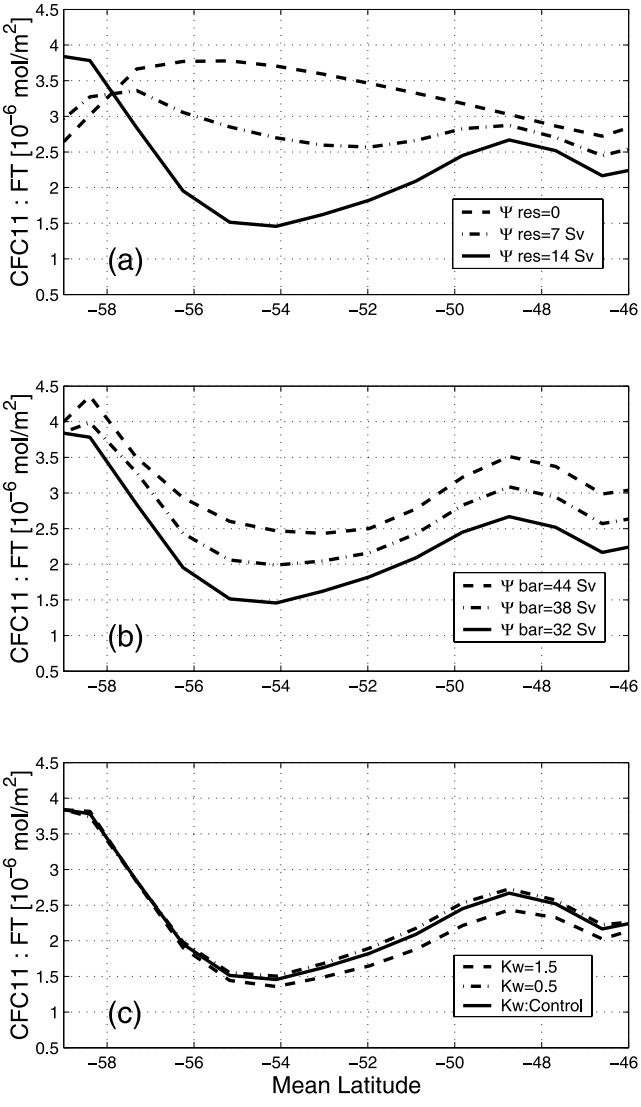

Figure 14. Modeled cumulative uptake of CFC-11 to 1990 in units of mol m^{-2}. The three panels illustrate sensitivity to (a) strength of the residual mean flow Ψ_{res}, (b) strength of the wind-driven, Eulerian mean flow, $\overline{\Psi}$ and, (c) gas transfer coefficient, K_W. Control runs are depicted by solid lines. The control simulation has Ψ_{res} = 14 Sv and $\overline{\Psi}$ = 32 Sv. The sensitivity experiments are made by multiplying buoyancy fluxes (adjusting Ψ_{res}), wind stress (adjusting $\overline{\Psi}$), or gas transfer coefficient, K_W, by constant factors (see legends).

flow (section 3). Figure 15a shows that the meridional profile of uptake is largely set by that of the surface wind forcing, but we observe enhanced uptake to the south of the ACC due to the upwelling of uncontaminated, deep waters. When the residual flow is switched off, $\Psi_{res} = 0$, the spatial pattern of the uptake more closely resembles the surface wind profile. The uptake to the north of 55°S is slightly increased when the residual flow, Ψ_{res}, is reduced because of changes in isopycnal diffusivity and surface distributions. Likewise, in Figure 15b, with greater $\overline{\Psi}$, the overall uptake is slightly increased due to enhanced isopycnal eddy diffusivity. However, the gross magnitudes and spatial patterns are strongly controlled by the meridional profile of gas transfer velocities, K_W (Figure 15c), and the sensitivity of modeled uptake is greater when the gas transfer coefficient is small. In summary, the modeled oceanic uptake of bomb-Δ^{14}C is most sensitive to the gas transfer coefficient, even though its regional distribution is sensitive to the residual flow. This is consistent with the simple scalings for the slow gas transfer regime.

5. Anthropogenic CO_2

[47] In the previous section we examined the fast- and slow-gas exchange limits that are appropriate for CFC-11 and bomb-Δ^{14}C, respectively. Of special interest, however, is the role of the Southern Ocean in the uptake of anthropogenic CO_2. The timescale for air-sea equilibration of CO_2

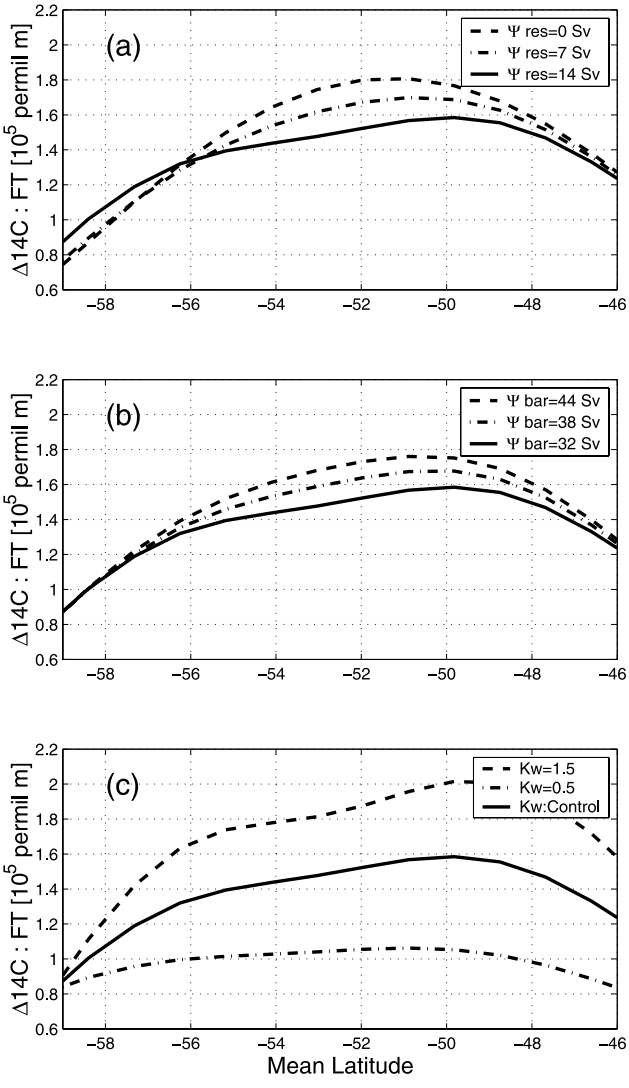

Figure 15. Cumulative uptake of bomb-$\Delta^{14}C$ to 1990 in units of permil m. Solid lines represent the control run. Sensitivities of (a) Ψ_{res}, (b) $\overline{\Psi}$, and (c) K_W are plotted as a function of the mean latitude of the streamline.

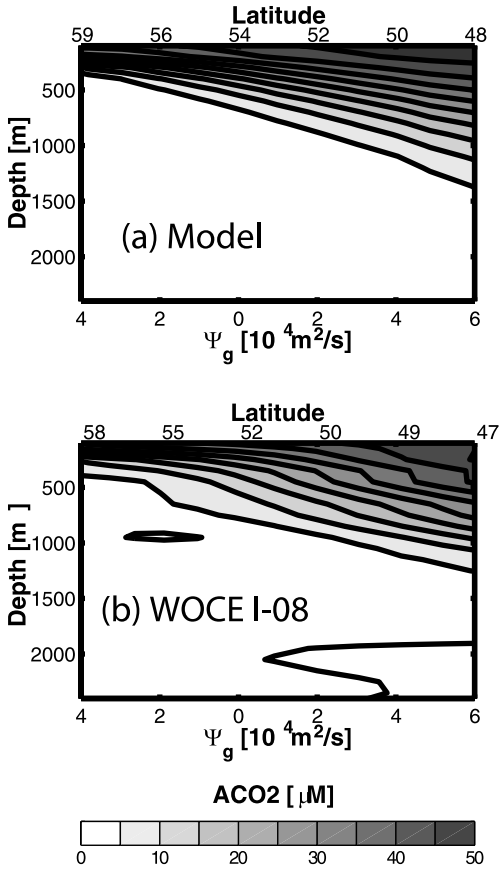

Figure 16. Distribution of anthropogenic CO_2 in the 1990s (a) from the streamline coordinate model and (b) derived from ocean observations [*Sabine et al.*, 1999] obtained from Global Ocean Data Analysis Project and reproduced with permission.

is on the order of 1 year, and so falls between the limit cases. Figure 16 shows the distribution of anthropogenic CO_2 in the 1990s from the streamline-averaged model and as derived from WOCE-era ocean observations. The observational estimate is from the Indian sector (90°E) of the gridded data of the Global Ocean Data Analysis Project using the ΔC^* method of *Sabine et al.* [1999]. There is a correspondence between the simulated and observed distributions in the streamline coordinate: In both cases the distribution lies somewhat between that of CFC-11 and bomb-$\Delta^{14}C$, as might be expected.

[48] Figure 17 shows the meridional distribution of the cumulative oceanic uptake of anthropogenic CO_2 in the model and its sensitivity to changes in physical forcing. It is sensitive to all of the physical parameters discussed here: buoyancy forcing (determining residual flow), wind stress forcing (determining eddy transfers), and air-sea gas transfer coefficient. Anthropogenic CO_2 has characteristics of both CFC-11 and bomb-$\Delta^{14}C$ since its gas exchange timescale lies somewhat between the two extreme cases. The gas transfer timescale for CO_2 is comparable to the timescale of physical transport, and so scaling suggests that the leading order balance must include both influences.

[49] There are two peaks in the modeled uptake of anthropogenic CO_2, around 58°S and 48°S in the control run, reminiscent of CFC-11 (compare Figures 14 and 17). What controls the pattern of the modeled oceanic uptake? The peak to the south of the ACC is due to upwelling of deep, uncontaminated water. The peak to the north of the ACC is due to enhanced isopycnal stirring, keeping surface concentrations low, and a stronger gas transfer coefficient there. Using simple theory and scaling analysis, we will illustrate two regimes of modeled cumulative uptake which are reflected in the regional model.

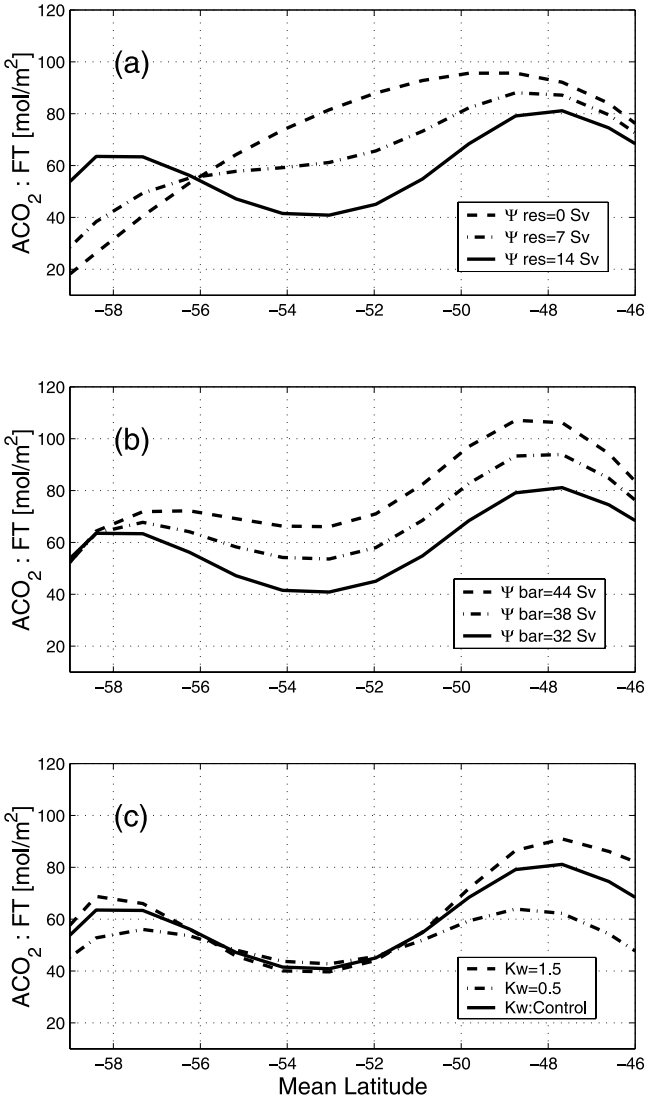

Figure 17. Cumulative uptake of anthropogenic CO_2 to 1990 in units of mol m^{-2}. Sensitivity to (a) residual mean flow, Ψ_{res}, (b) wind-driven, Eulerian mean flow, $\overline{\Psi}$, and (c) gas transfer coefficient, K_W. The model results are plotted as a function of the mean latitude of streamlines. Control runs are depicted by solid lines. The control simulation has Ψ_{res} = 14 Sv and $\overline{\Psi}$ = 32 Sv. The sensitivity experiments are made by multiplying buoyancy fluxes (to control Ψ_{res}), wind stress (to control $\overline{\Psi}$), and gas transfer coefficient, K_W, by constant factors (see legends).

[50] First, to the south of the ACC (around 58°S), there is large-scale upwelling as shown in Figure 6. The upwelling deep waters are essentially free of anthropogenic CO_2, driving surface partial pressures down. We hypothesize that the entrainment term is likely to control the air-sea flux in that region and consider a local balance between entrainment and air-sea fluxes. The upwelling waters are depleted in transient tracers ($C_{th} \ll C$), so a simple expression describes the local uptake,

$$\frac{w_{res}}{h} C \sim -\lambda (C - C_{at}). \tag{16}$$

We define a non-dimensional parameter, $W \equiv \frac{w_{res}}{h\lambda}$, which represents the competition between the rate of large-scale upwelling and the rate of gas transfer. Solving for C and for the uptake, $F = -\lambda h(C - C_{at})$, we find

$$C \sim C_{at}(1 + W)^{-1}, \tag{17}$$

$$F \sim \lambda\, h\, C_{at} \left(\frac{W}{1 + W} \right). \tag{18}$$

The relationships for anthropogenic CO_2 fall between the limit cases of CFC-11 and bomb-Δ^{14}C. In the fast gas exchange limit, $W \ll 1$, equations (17) and (18) become identical to equations (10) and (12). Similarly, in the slow gas exchange limit, $W \gg 1$, equation (18) becomes identical to equation (15). The concentration and uptake of anthropogenic CO_2 depend on the balance between the upwelling rate and the gas transfer coefficient. To the south of the ACC, the uptake rate is thus closely related to Ψ_{res}, as illustrated by the sensitivity experiments in Figure 14a. A 50% decrease in Ψ_{res} leads to a 40% decrease in the cumulative uptake, consistent with equation (18) when $W \sim 0.3$. Figure 16 shows that the surface concentration to the south of the ACC is indeed low, partly due to the large-scale upwelling of deep waters with low anthropogenic CO_2 concentration there. However, the latitudinal variation of the Buffer factor also contributes to the low anthropogenic CO_2 concentration in this region. The effective solubility of anthropogenic CO_2 depends on both solubility of CO_2 and the Buffer factor, reflecting the seawater carbonate chemistry. The net effect of these influences is an increase in effective solubility of anthropogenic CO_2 with temperature. Thus, warmer water has greater CO_2 uptake capacity at a given rate of atmospheric pCO_2 increase.

[51] A second anthropogenic CO_2 peak emerges to the north of the ACC at around 48°S where eddy transfers are vigorous. Here we can identify a second regime in which there is a local balance between isopycnal stirring and air-sea fluxes:,

$$\frac{K s_\rho}{h} \left(\frac{\partial C}{\partial y} \right)_{\rho, -h} \sim -\lambda (C - C_{at}). \tag{19}$$

Caldeira and Duffy [2000] simulated anthropogenic CO_2 uptake in the Southern Ocean using a GCM, and described the northward isopycnal stirring of CO_2 as indicated by equation (19). Using equations (5) and (6) to relate eddy-induced flow and isopycnic eddy diffusivity, we define a non-dimensional parameter, $D \equiv \frac{\Psi_{eddy}}{\lambda h L}$, which represents the competition between the rate of isopycnal stirring and the rate of gas transfer. We solve for C and the uptake, $F = -\lambda h(C - C_{at})$,

$$C \sim C_{at}(1 + D)^{-1}, \tag{20}$$

$$F \sim \lambda\, h\, C_{at} \left(\frac{D}{1 + D} \right). \tag{21}$$

These relationships are in a form similar to equations (17) and (18), except here D is controlled by Ψ_{eddy} and not Ψ_{res}. Again, these relationships become identical to the solutions for uptake of CFC-11 and bomb-Δ^{14}C in the fast and slow gas exchange limits, respectively. The rate of uptake is controlled by the competition between the rate of gas transfer and Ψ_{eddy}. Figure 17b shows that the modeled, overall magnitude of the cumulative uptake does indeed increase with stronger wind stress (which leads to stronger eddy transfers if buoyancy distribution and fluxes are held constant). Contrast this with Figure 17a, in which the cumulative uptake decreases with stronger buoyancy flux.

[52] The cumulative uptake of anthropogenic CO_2 increases with faster gas transfer coefficient, but the sensitivity is not uniform in space. The regions of strong uptake around 58°S and 48°S are sensitive to the gas transfer coefficient, while other regions are not (Figure 17c). This is consistent with equations (18) and (21), which suggest that the cumulative uptake in these peak regions should increase with faster gas transfer coefficient. At high values of gas transfer coefficient, sensitivity decreases since surface waters move closer to saturation and the system shifts to the fast gas exchange limit.

[53] The uptake of anthropogenic CO_2 is sensitive to both the parameterization of the gas transfer coefficient and the climatological distribution of buoyancy fluxes that determines the residual flow. Hence the uncertainty in the modeled uptake of anthropogenic CO_2 is greater than that of CFC-11 and bomb-Δ^{14}C, which represent limit cases that are insensitive to gas transfer coefficient and buoyancy fluxes (residual flow), respectively. The differences between published climatologies (Figure 5) suggest that the major sources of uncertainty lie in the buoyancy fluxes (>50%) and residual flow, with smaller differences between wind climatologies and hence the gas transfer coefficient (~10%). If we simply assume that these uncertainties in the forcing linearly project onto the uptake, we expect an uncertainty in modeled uptake of anthropogenic CO_2 on the order of 60%, simply because of uncertainties in the surface physical forcing data sets.

[54] In a comparison of modeled uptake of anthropogenic CO_2 using several GCMs, *Orr et al.* [2001] find model-to-model differences on the order of 70% in the Southern Ocean. In that study (OCMIP), a consistent profile of the gas transfer coefficient was used by all models, but the buoyancy forcing and parameterization of subgrid-scale eddies differ between the models. Our analysis suggests that much of the model-to-

model difference in the Southern Ocean CO_2 fluxes in the OCMIP models could simply be attributable to the choice of surface boundary conditions for buoyancy and the resulting differences in Ψ_{res} in the models that use *Gent and McWilliams* [1990] type eddy transfer parameterizations. Those models, which do not explicitly account for eddy-induced advection, might be expected to have introduced an uncertainty of O(1) in Ψ_{res} in the Southern Ocean where eddy-induced flow plays a dominant role.

[55] In Figure 17, the cumulative uptake of anthropogenic CO_2 south of 56°S increases with stronger buoyancy fluxes, but it decreases to the north, indicating that the net CO_2 uptake has only a weak dependence on the buoyancy fluxes despite strong regional sensitivities. The spatially integrated cumulative uptake (between 60°S and 46°S) is 27.8 PgC in the control run, increasing by less than 10% when Ψ_{res} is reduced by 50%, although the spatial patterns of the uptake are very different (Figure 17a). This is due to a partial compensation between advection and eddy stirring. The diffusive transport is reduced when the residual circulation is intense, and vice versa, because the isopycnal tracer gradient decreases with stronger residual flow. Overall, the net uptake is smaller with greater Ψ_{res}, as suggested by equation (21).

6. Summary and Discussion

[56] We have developed simple scalings that relate the Southern Ocean uptake of transient tracers to the physical forcing. The scalings are rooted in residual mean theory and a streamline-averaged view of the ACC. We have considered the influence of surface buoyancy fluxes, wind stress, and gas transfer coefficient on three transient tracers, namely, CFC-11, bomb-$\Delta^{14}C$, and anthropogenic CO_2. In addition to scaling arguments, we have developed an explicit two-dimensional (streamline-averaged) numerical model of the meridional tracer transport in the vicinity of the ACC, again rooted in residual mean theory. We use the numerical model to test the simple scalings and to perform sensitivity studies illustrating the uncertainties in modeled ocean tracer uptake due to uncertainties in forcing data sets.

[57] The relationships of ocean tracer distributions and oceanic uptake to the physical forcing are sensitive to the timescale of air-sea gas exchange. There is a large separation in the respective gas exchange timescales of CFC-11 and bomb-$\Delta^{14}C$, so they have very different sensitivities to the three physical parameters.

6.1. Tracer Distributions

[58] Since CFC-11 equilibrates rapidly, its surface distribution reflects solubility and atmospheric partial pressure but is not significantly impacted by the residual flow or isopycnal mixing. Bomb-$\Delta^{14}C$ equilibrates slowly, and the surface distribution reflects the upwelling of uncontaminated deep waters and the accumulation of tracer in the northward flowing residual circulation. Hence the contrasting gradients of CFC-11 and bomb-$\Delta^{14}C$ in the surface Southern Ocean reflect the strength of the residual flow, which cannot be directly observed. It also provides a useful diagnostic by which the strength of the residual flow in numerical models may be compared. In the thermocline, however, both tracers simply reflect advection and mixing down from the surface. The ability of the streamline-averaged model to qualitatively reproduce observed features provides support for the application of the residual mean theoretical approach.

6.2. Ocean Uptake

[59] The behavior of CFC-11 is well represented by the fast gas exchange limit in the mixed layer tracer balance. The oceanic uptake of CFC-11 largely reflects upper ocean transport processes (illustrated in Figure 10). The spatial pattern of the cumulative air-sea flux is sensitive to the strength of the residual flow that controls the rate at which deep, uncontaminated waters are supplied to the surface. The residual flow is, in turn, controlled by the pattern of air-sea buoyancy fluxes, since the heat budget and water mass transformation rates must be consistent. Isopycnal eddy transfer also plays a significant role in promoting uptake of CFC-11 by keeping surface water partial pressures low. The vigor of eddy stirring is largely controlled by the surface wind stress, since eddy activity must, to zero order, counteract the wind-driven Deacon Cell. In contrast, bomb-$\Delta^{14}C$ reflects a slow gas exchange limit. As a consequence, the uptake of bomb-$\Delta^{14}C$ is mainly controlled by the gas transfer coefficient (illustrated in Figure 11). The pattern of uptake fundamentally depends on the profile of surface wind speed. Variations in isopycnal eddy diffusivity and residual flow can also impact the uptake of bomb-$\Delta^{14}C$, but their effects are somewhat moderate.

[60] In this idealized model, while the spatial pattern of the cumulative uptake of CFC-11 and anthropogenic CO_2 are highly sensitive to residual flow, Ψ_{res}, the spatially integrated uptake is not. It has been noted that the uptake of anthropogenic CO_2 in the three-dimensional, general circulation and biogeochemistry models of the OCMIP study, show considerable variations in spatial pattern in the Southern Ocean [*Orr et al.*, 2001], and yet, the simulated global uptake from those models agrees relatively well (to within 20%). We suggest that model-to-model differences in the spatial patterns of the anthropogenic CO_2 uptake are likely due to the differences in the representation of Ψ_{res} (in those models with GM90-type eddy transfer parameterizations).

[61] The uptake and transport of tracers is sensitive to the water mass transformations and residual flow, Ψ_{res}, which must be consistent with the surface buoyancy distribution and buoyancy fluxes [*Marshall*, 1997]. However, climatological buoyancy fluxes in the Southern Ocean presently have large uncertainties, witnessed by the variations between data climatologies (Figure 5). Hence, even if the buoyancy fluxes are imposed in numerical ocean models, this uncertainty is reflected in the modeled tracer uptake. Our sensitivity studies suggest that this factor alone is sufficient to explain much of the model-to-model difference in Southern Ocean anthropogenic CO_2 uptake in the OCMIP models. (Although this may be a significant factor, we do not suggest that it is the only one: The OCMIP models differ greatly in choice of subgrid-scale eddy transfer parameterizations and physical boundary conditions at the surface).

[62] In this study we applied spatially varying isopycnal eddy transfer coefficients, following *Visbeck et al.* [1997], in contrast to most current general circulation and biogeochemistry models, in which spatially homogeneous isopycnal mixing coefficients are assumed. If the diffusivity is assumed to be constant, the isopycnal slope is linearly related to the wind stress. The isopycnal eddy flux at the base of the mixed layer in equation (8) scales with the product of the isopycnal slope and the eddy diffusivity, and so the diffusive transport responds linearly to the wind stress. It is coincidental that the isopycnal eddy flux has linear dependence on the wind stress for both cases: Eddy parameterization based on uniform diffusivity and that based on spatially varying diffusivity of *Visbeck et al.* [1997] results in the same linear sensitivity of tracer uptake to the wind stress.

[63] Thus far, we have treated surface wind stress and gas transfer coefficients as independent variables in order to illustrate model sensitivities in a transparent way. In reality, both depend on the wind speed at the sea surface, and are not independent. A stronger surface wind will enhance both the uptake of CFC-11 and that of bomb-Δ^{14}C. However, different processes control the increase in uptake of these two tracers. The uptake of CFC-11 is enhanced by the increase in isopycnal eddy diffusion, and the uptake of bomb-Δ^{14}C increases because of the greater gas transfer velocities. For anthropogenic CO_2, both isopycnal diffusivity and gas transfer velocities will enhance uptake, since its intermediate equilibration timescale make it sensitive to both effects.

[64] The models and scalings presented here are deliberately idealized and simplified to provide clearer insights. However, this leads to the omission of some processes that are also significant in the region. Notably, the polar regions of the Southern Ocean are partially ice covered, affecting buoyancy and tracer fluxes. Also, there are regions of significant deep water formation also affecting the regional uptake of tracers by the ocean. These processes are certainly worthy of closer study and are omitted here to focus on processes associated with upwelling regions and the formation of intermediate and mode waters.

[65] In brief, we have applied residual mean theory to develop scalings and idealized numerical models of the uptake of transient tracers in the Southern Ocean. The streamline-averaged numerical model captures the observed distributions of CFC-11, bomb-Δ^{14}C, and anthropogenic CO_2 and their relationships to one another, suggesting that there is a residual overturning flow of about 14 Sv in the Southern Ocean. Sensitivity studies with the model suggest that the uncertainties in air-sea buoyancy fluxes in current climatologies impose significant uncertainty in estimates of Southern Ocean uptake of anthropogenic CO_2 from current circulation and biogeochemistry models that are driven by, or seek to be consistent with, the climatological fluxes.

Appendix A: Aquatic Chemistry of CFC-11

[66] We briefly describe chemical component of the numerical model. We calculate the solubility of CFC-11 following *Warner and Weiss* [1985]. The equilibrium concentration of CFC-11 is given as

$$C_{at} = k_{CFC-11} pCFC. \tag{A1}$$

The air-sea flux of CFC-11 is parameterized such that the air-sea flux (positive into the ocean) is

$$F = K_W (C_{at} - C). \tag{A2}$$

The gas transfer coefficient, K_W, is parameterized following *Wanninkhof* [1992].

Appendix B: Aquatic Chemistry of CO_2

[67] Chemical equilibrium is assumed for carbonate chemistry in the model, and the equilibrium constants are calculated following *Millero* [1995]. In order to calculate the effective solubility for anthropogenic CO_2, we used the fact that variations in saturated DIC concentration are related to variations in partial pressure of CO_2 through the Buffer factor.

$$\delta DIC = \frac{DIC}{B_u \, pCO_2} \delta pCO_2, \tag{B1}$$

where DIC and pCO_2 are the concentration and the partial pressure in the preindustrial sea water. We prescribe the anthropogenic perturbation in the partial pressure of CO_2, δpCO_2, to the values shown in Figure 1. Here δDIC represents the anthropogenic perturbation in the equilibrium DIC, which would be the anthropogenic component of the DIC concentration if the surface water is saturated with the atmospheric pCO_2. Thus the effective solubility of anthropogenic CO_2 can be calculated with preindustrial values of DIC, pCO_2, and B_u, assuming that the Buffer factor remains constant for the range of perturbation in pCO_2.

[68] The saturated DIC concentration is determined as follows:

$$DIC_{at} = k_{CO_2} \left[1 + \frac{K_1}{[H^+]} + \frac{K_1 K_2}{[H^+]^2} \right] pCO_2^{at}, \tag{B2}$$

where k_{CO_2} is the solubility of CO_2 in sea waters [*Weiss*, 1974]. Here K_1 and K_2 are equilibrium constants for bicarbonate ions and carbonate ions [*Mehrback et al.*, 1973]. In order to determine the relationship between the DIC concentration and the partial pressure of CO_2, the pH of the sea water must be determined. We calculate the pH of the surface water by an iterative method assuming that (1) the preindustrial atmospheric partial pressure, pCO_{20}, is equal to 278 ppmv, and (2) temperature, salinity, and alkalinity of the surface water are prescribed. For temperature and salinity, we use streamline-averaged Levitus climatology. For alkalinity, we assume a spatially uniform concentration of 2300 μeq kg^{-1}. $[H^+]$ is solved using Newton's method, and the resulting equilibrium DIC concentration, DIC_0, is used to parameterize the effective solubility of anthropogenic CO_2. The Buffer factor, B_u, is also calculated by perturbing pCO_2 and recalculating DIC

from equation (B2). DIC_0 and B_u are used to define C_{at} for anthropogenic CO_2.

$$C_{at} = \frac{DIC_0}{B_u\, pCO_2}(pCO_{20} - 278\ \text{ppmv}). \tag{B3}$$

The gas exchange timescale for CO_2 is different from that of CFC-11 because of the carbonate chemistry [*Broecker and Peng*, 1974]; see Table 1. The air-sea flux of anthropogenic CO_2 is parameterized as

$$F = \frac{K_W\, pCO_{20}}{DIC_0\, B_u}(C_{at} - C). \tag{B4}$$

[69] **Acknowledgments.** Thanks are owed to Bob Key for stimulating suggestions and to an anonymous reviewer whose comments helped to improve this manuscript. We are grateful for support from the Office of Polar Programs at NSF. M. J. F. is also grateful for support from NSF grant OCE-0136609.

References

Andrews, D. G., and M. E. McIntyre (1976), Planetary waves in horizontal and vertical shear: The generalized Eliassen-Palm relation and the zonal mean acceleration, *J. Atmos. Sci.*, *33*, 2031–2048.

Broecker, W. S., and T. H. Peng (1974), Gas exchange rates between air and sea, *Tellus*, *26*, 21–35.

Caldeira, K., and P. B. Duffy (2000), The role of the Southern Ocean in uptake and storage of anthropogenic carbon dioxide, *Science*, *287*, 620–622.

da Silva, A., A. C. Young, and S. Levitus (1994), *Atlas of Surface Marine Data 1994*, vol. 1, *Algorithms and Procedures*, *NOAA Atlas NESDIS 6*, Natl. Oceanic and Atmos. Admin., Silver Spring, Md.

Dutay, J. C., et al. (2002), Evaluation of ocean model ventilation with CFC-11: Comparison of 13 global ocean models, *Ocean Modell.*, *4*, 89–120.

Gent, P. R., and J. C. McWilliams (1990), Isopycnal mixing in ocean circulation models, *J. Phys. Oceanogr.*, *20*, 150–155.

Gille, S. T. (1994), Mean sea-surface height of the antarctic circumpolar current from GEOSAT data: Method and application, *J. Geophys. Res.*, *99*(C9), 18,255–18,273.

Gruber, N. (1998), Anthropogenic CO_2 in the Atlantic Ocean, *Global Biogeochem. Cycles*, *12*(1), 165–191.

Gruber, N., J. L. Sarmiento, and T. F. Stocker (1996), An improved method for detecting anthropogenic CO_2 in the ocean, *Global Biogeochem. Cycles*, *10*(4), 809–837.

Held, I. M., and T. Schneider (1999), The surface branch of the zonally averaged mass transport circulation in the troposphere, *J. Atmos. Sci.*, *56*, 1688–1697.

Johnson, G. C., and H. L. Bryden (1989), On the size of the Antarctic Circumpolar Current, *Deep Sea Res.*, *36*, 39–53.

Josey, S., E. Kent, and P. Taylor (1999), New insights into the ocean heat budget closure problem from analysis of the SOC air-sea flux climatology, *J. Clim.*, *12*(9), 2856–2880.

Kalnay, E., et al. (1996), The NCEP/NCAR 40-yr reanalysis project, *Bull. Am. Meteorol. Soc.*, *77*, 437–471.

Karsten, R., and J. C. Marshall (2002), Constructing the residual circulation of the Antarctic Circumpolar Current from observations, *J. Phys. Oceanogr.*, *32*, 3315–3327.

Karsten, R., H. Jones, and J. C. Marshall (2002), The role of eddy transfer in setting the stratification and transport of a Circumpolar Current, *J. Phys. Oceanogr.*, *32*, 39–54.

Keeling, R. F., R. P. Najjar, M. L. Bender, and P. P. Tans (1993), What atmospheric oxygen can tell us about the global carbon-cycle, *Global Biogeochem. Cycles*, *7*(1), 37–67.

Levitus, S., and T. Boyer (1994), *World Ocean Atlas 1994*, vol. 4, *Temperature*, *NOAA Atlas NESDIS 4*, Natl. Oceanic and Atmos. Admin., Silver Spring, Md.

Marshall, D. (1997), Subduction of water masses in an eddying ocean, *J. Mar. Res.*, *55*, 201–222.

Marshall, J. C., and T. Radko (2003), Residual mean solutions for the Antarctic Circumpolar Current and its associated overturning circulation, *J. Phys. Oceanogr.*, *33*, 2341–2354.

Marshall, J., C. Hill, L. Perelman, and A. Adcroft (1997a), Hydrostatic, quasi-hydrostatic, and non-hydrostatic ocean modeling, *J. Geophys. Res.*, *102*(C3), 5733–5752.

Marshall, J., A. Adcroft, C. Hill, and L. Perelman (1997b), A finite-volume, incompressible Navier Stokes model for studies of the ocean on parallel computers, *J. Geophys. Res.*, *102*(C3), 5753–5766.

Matear, R. J. (2001), Effects of numerical advection schemes and eddy parameterizations on ocean ventilation and oceanic anthropogenic CO_2 uptake, *Ocean Modell.*, *3*, 217–248.

McNeil, B. I., R. J. Matear, R. M. Key, J. L. Bullister, and J. L. Sarmiento (2003), Anthropogenic CO_2 uptake by the ocean based on the global chlorofluorocarbon data set, *Science*, *299*, 235–239.

Mehrback, C., C. H. Culberson, J. E. Hawley, and R. M. Pytkowicz (1973), Measurement of the apparent dissociation constants of carbonic acid in seawater at atmospheric pressure, *Limnol. Oceanogr.*, *18*, 897–907.

Millero, F. J. (1995), Thermodynamics of the carbon dioxide system in the oceans, *Geochim. Cosmochim. Acta*, *59*(4), 661–677.

Murnane, R. J., J. L. Sarmiento, and C. LeQur (1999), Spatial distribution of air-sea CO_2 fluxes and the interhemispheric transport of carbon by the oceans, *Global Biogeochem. Cycles*, *13*(2), 287–305.

Orr, J. C., et al. (2001), Estimates of anthropogenic carbon uptake from four three-dimensional global ocean models, *Global Biogeochem. Cycles*, *15*(1), 43–60.

Robitaille, D. Y., and A. J. Weaver (1995), Validation of subgrid-scale mixing schemes using CFCs in a global ocean model, *Geophys. Res. Lett.*, *22*(21), 2917–2920.

Rubin, S. I., and R. M. Key (2002), Separating natural and bomb-produced radiocarbon in the ocean: The potential alkalinity method, *Global Biogeochem. Cycles*, *16*(4), 1105, doi:10.1029/2001GB001432.

Sabine, C., R. M. Key, F. J. Millero, A. Poisson, J. L. Sarmiento, D. W. R. Wallace, and C. D. Winn (1999), Anthropogenic CO_2 inventory of the Indian Ocean, *Global Biogeochem. Cycles*, *13*(1), 179–198.

Solomon, H. (1971), On the representation of isentropic mixing in ocean circulation models, *J. Phys. Oceanogr.*, *1*, 233–234.

Speer, K., S. R. Rintoul, and B. Sloyan (2000), The diabatic deacon cell, *J. Phys. Oceanogr.*, *30*, 3212–3222.

Visbeck, M., J. Marshall, T. Haine, and M. Spall (1997), Specification of eddy transfer coefficients in coarse-resolution ocean circulation models, *J. Phys. Oceanogr.*, *27*, 381–402.

Wanninkhof, R. (1992), Relationship between wind-speed and gas-exchange over the ocean, *J. Geophys. Res.*, *97*(C5), 7373–7382.

Warner, M. J., and R. F. Weiss (1985), Solubilities of Chlorofluorocarbon 11 and Chlorofluorocarbon 12 in water and sea water, *Deep Sea Res.*, *32*, 1485–1497.

Weiss, R. F. (1974), Carbon dioxide in water and sea water: The solubility of a non-ideal gas, *Mar. Chem.*, *2*, 203–215.

M. Follows, T. Ito, and J. Marshall, Program in Atmospheres Oceans and Climate, Department of Earth, Atmospheric and Planetary Sciences, Massachusetts Institute of Technology, 54-1511, Cambridge MA 02139, USA. (ito@ocean.mit.edu)